ATM–dependent phosphorylation of CHD7 regulates morphogenesis-coupled DSB stress response in fetal radiation exposure

Asao Noda*, Kaori Muramoto, and Shuji Mishima
Department of Molecular Biosciences, Radiation Effects Research Foundation, Minami-ku, Hiroshima City, Hiroshima 732-0815, Japan

ABSTRACT **Following radiation exposure, unrepaired DNA double-strand breaks (DSBs) persist to some extent in a subset of cells as residual damage; they can exert adverse effects, including late-onset diseases. In search of the factor(s) that characterize(s) cells bearing such damage, we discovered ataxia-telangiectasia mutated (ATM)-dependent phosphorylation of the transcription factor chromodomain helicase DNA binding protein 7 (CHD7). CHD7 controls the morphogenesis of cell populations derived from neural crest cells during vertebrate early development. Indeed, malformations in various fetal bodies are attributable to CHD7 haploinsufficiency. Following radiation exposure, CHD7 becomes phosphorylated, ceases promoter/enhancer binding to target genes, and relocates to the DSB-repair protein complex, where it remains until the damage is repaired. Thus, ATM-dependent CHD7 phosphorylation appears to act as a functional switch. As such stress responses contribute to improved cell survival and canonical nonhomologous end joining, we conclude that CHD7 is involved in both morphogenetic and DSB-response functions. Thus, we propose that higher vertebrates have evolved intrinsic mechanisms underlying the morphogenesis-coupled DSB stress response. In fetal exposure, if the function of CHD7 becomes primarily shifted toward DNA repair, morphogenic activity is reduced, resulting in malformations.**

Monitoring Editor
Dennis Discher
University of Pennsylvania

Received: Oct 3, 2022
Revised: Feb 23, 2023
Accepted: Mar 3, 2023

This article was published online ahead of print in MBoC in Press (http://www.molbiolcell.org/cgi/doi/10.1091/mbc.E22-10-0450) on March 8, 2023.

Author contributions: A.N. designed the study and performed cell culture, immunostaining, and mouse experiments. K.M. and S.M. performed immunoprecipitation and Western blot analyses. S.M. created CHD7 and 53BP1 KO cells. All authors contributed to writing the manuscript and approving the final version of the manuscript.

*Address correspondence to: Asao Noda (asnoda@rerf.or.jp).

Abbreviations used: ATM, ataxia telangiectasia mutated; CHARGE, coloboma of the eye, heart defects, atresia of the choanae, retardation of growth/development, genital or urinary abnormalities, and ear abnormalities; CHD7, chromodomain helicase DNA binding protein 7; DSB, double-strand break; ChIP, chromatin immunoprecipitation; DKO, double knockout; FLAG tag, peptide sequence DYKDDDDK tag; GFP, green fluorescent protein; HPRT, hypoxantine-guanine phosphoribosyltransferase; KD, knockdown; KO, knockout; LCR, locus control region; NHEJ, nonhomologous end joining; WT, wild type.

INTRODUCTION

Vertebrate embryogenesis is a sophisticated process involving precise timelines for cell division and differentiation, the driving force of which includes programmed changes in chromatin structure and corresponding transcription factors that induce the expression of key proteins for cell division, locomotion of cell populations for morphogenesis, and differentiation. A classical question of developmental biology concerns the mechanisms underlying development, which can be clarified through cell lineage tracking. In current molecular biology studies, methods to investigate chromatin modification and transcription factor expression at single-cell resolution are applied (He *et al*., 2020; Fan and Huang, 2021).

Among the transcription factors that control embryogenesis, chromodomain helicase DNA binding protein 7 (CHD7) (Woodage *et al*., 1997; Vissers *et al*., 2004; Basson and van Ravenswaaij-Arts, 2015) regulates the expression of many genes by binding to targeted gene promoter/enhancer sequences to form a specific

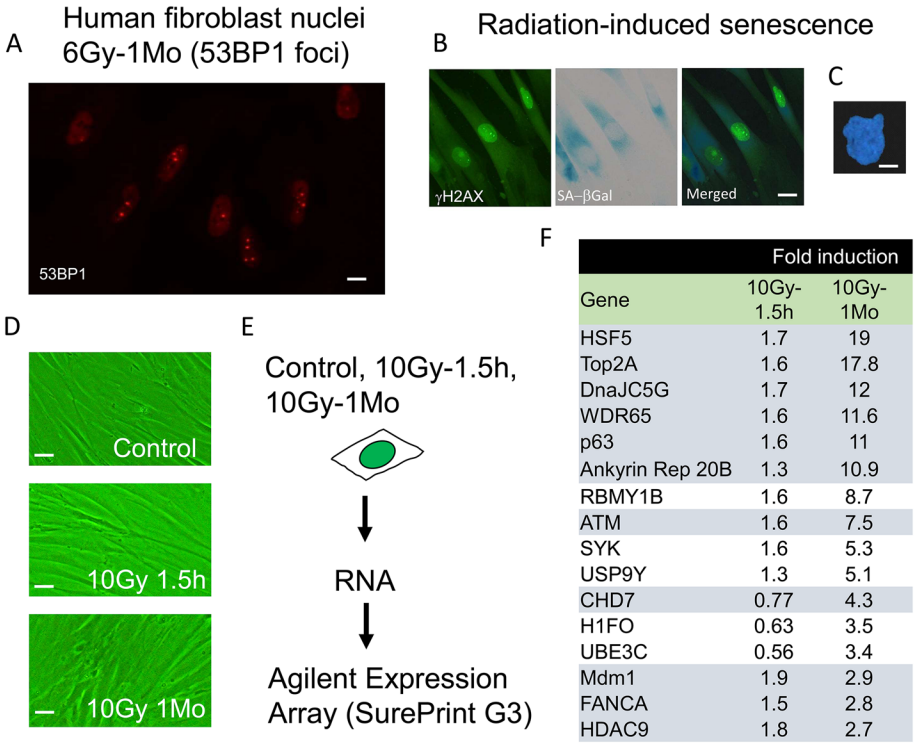

F

	Fold induction	
Gene	10Gy-1.5h	10Gy-1Mo
HSF5	1.7	19
Top2A	1.6	17.8
DnaJC5G	1.7	12
WDR65	1.6	11.6
p63	1.6	11
Ankyrin Rep 20B	1.3	10.9
RBMY1B	1.6	8.7
ATM	1.6	7.5
SYK	1.6	5.3
USP9Y	1.3	5.1
CHD7	0.77	4.3
H1FO	0.63	3.5
UBE3C	0.56	3.4
Mdm1	1.9	2.9
FANCA	1.5	2.8
HDAC9	1.8	2.7

FIGURE 1: Characterization of human diploid fibroblast cells bearing radiation-induced unrepaired DSBs by cell morphology and specific gene expression. (A) Unrepaired DSB foci in the nucleus as revealed by 53BP1 antibody staining. They tend to form pairs. The image shows cell nuclei 1 mo after the 6 Gy exposure. Scale bar, 20 μm. (B) Such DSB foci also carry γH2AX proteins, and the cells often exhibit SA-β-Gal positivity and (C) dysmorphic nuclei by DAPI staining, as previously reported (Noda *et al.*, 2012, 2015a). Scale bar, 5 μm. (D) Quiescent culture of 10 Gy-1 Mo cells carrying unrepaired DSBs appeared to be healthy and stable. (E) RNA was extracted from the control, 10 Gy-1.5 h, and 10 Gy-1 Mo cells and subjected to Agilent expression array analysis. (F) Genes that showed less than twofold up- or down-regulation at 10 Gy-1.5 h and then significant up-regulation at 10 Gy-1 Mo.

transcription complex (Schnetz *et al.*, 2009, 2010), where the CHD7 partners vary among cell types during development (Martin, 2010; Engelen *et al.*, 2011; Feng *et al.*, 2017; Whittaker *et al.*, 2017). For instance, in neuronal stem cells, CHD7 binds SOX2 to target promoter/enhancer sequences in *JAG1*, *GIL3*, and *MYCN* to induce gene expression. Hence, depending on the tissues, various partners, including Nanog1, p300, PBAF, BAF, BRG1, PPAR, PARP, WDR5, and SMADs, join the transcription complex (Liu *et al.*, 2014). Moreover, binding of H3K4Me3, H3K27Ac, and HDAC1/2 has also been reported (Schnetz *et al.*, 2009; Feng *et al.*, 2017; Rother *et al.*, 2020). ChIP sequencing has further identified myriad CHD7-binding sequences through the genome (Schnetz *et al.*, 2009, 2010). Hence, by changing the target, CHD7 functions to selectively control time-dependent gene expression by altering chromatin accessibility (Yao *et al.*, 2020).

In early embryos, CHD7 can induce morphogenesis and differentiation of neural crest–derived cell populations. Given that neural crest cells differentiate into various tissues (Bajpai *et al.*, 2010; Pauli *et al.*, 2017; Yan *et al.*, 2020), a decrease in CHD7 protein abundance, or its dysfunction, causes abnormal heart and neurosensory organ development, resulting in neonatal deformities (Sperry *et al.*, 2014; Payne *et al.*, 2015). In humans, heterozygous CHD7 loss of function results in multiple congenital malformations known as CHARGE syndrome (coloboma of the eye, heart defects, atresia of the choanae, retardation of growth/development, genital or urinary abnormalities, and ear abnormalities) (Vissers *et al.*, 2004; Bosman *et al.*, 2005; Zentner *et al.*, 2010). Meanwhile, its homozygous mutants in mice are lethal to embryos (Hurd *et al.*, 2007; Layman *et al.*, 2009; Zentner *et al.*, 2010; Basson and van Ravenswaaij-Arts, 2015), indicating that *CHD7* is a typical haploinsufficient gene.

Radiation exposure interferes with early embryogenesis, resulting in embryonic death or congenital abnormality (Hall, 1994; ICRP, 2003). Embryonic death is primarily induced during the preimplantation stage, whereas malformation occurs preferentially in the organogenic stage. In particular, the tumor suppressor protein p53 is intricately involved in radiation injury and embryonic malformation. However, p53 is also a transcription factor that has a central role in controlling cell cycle progression through checkpoint activation and eliminating abnormal cells in early embryos by inducing their apoptotic death. Therefore, p53 plays a passive role in preventing malformation (Norimura *et al.*, 1996; Nomoto *et al.*, 1998). Are there any active factors that secure normal development? If such a factor exists, it will promote the recovery of damaged cells in the DNA damage stress response. However, the embryo has no additional time in the predetermined morphogenic movement to briefly stop cell division and promptly repair the damage via conventional checkpoint signals, implying that an alternate mechanism is required.

The current study sought to elucidate the biological effects of unrepaired DNA damage. While characterizing cells bearing unrepaired DNA damage, we observed that CHD7 underwent ataxia-telangiectasia mutated (ATM)-dependent phosphorylation. This protein was quickly phosphorylated upon irradiation and then released from the original transcription regulatory position and localized at double-strand break (DSB) sites, where it stayed until the damage was repaired. This dual function of CHD7 in morphogenesis and damage response implies that morphogenesis and DNA repair are coupled during early embryonic development. For strict progression of development, vertebrate organisms may have evolved mechanisms to simultaneously tackle morphogenesis and DSB repair to maintain the timetable of development. Herein, we discuss the universality of this coupling of the genome damage response mechanism and morphogenesis.

RESULTS

Identifying specific genes with increased expression in cells bearing unrepaired DSBs

We previously detected unrepaired DSBs as persistent DSB foci (DSB-repair protein complexes) in nuclei 1 mo (month) post–radiation exposure, which constituted nearly 1% of the originally formed DSB foci (Noda *et al.*, 2012, 2018), with pairs in each nucleus appearing as torn-off DNA end structures (Figure 1A and data in our previous studies). These cells exhibited a senescent phenotype (Figure 1B), often forming dysmorphic nuclear membrane structures

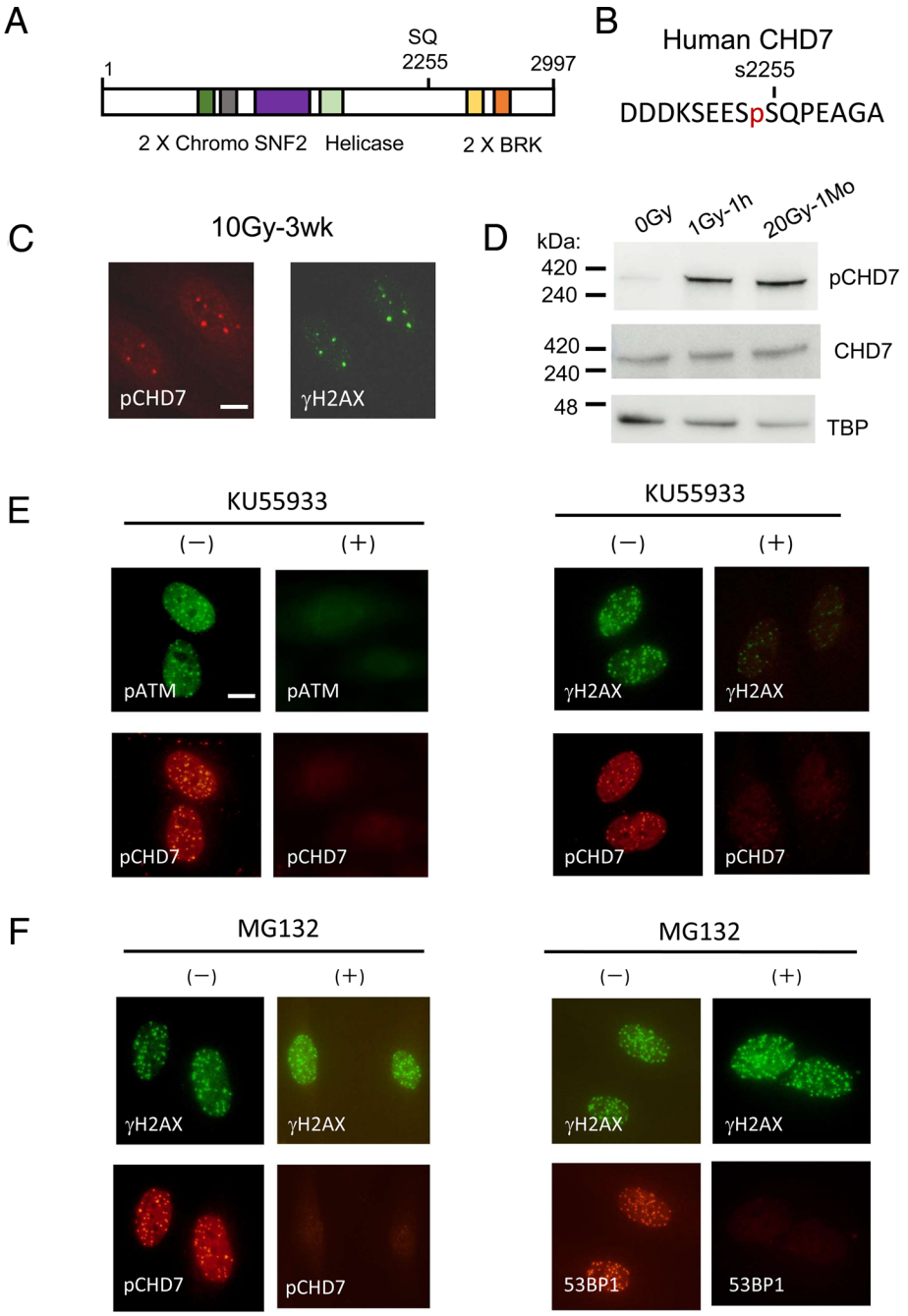

FIGURE 2: Detection of radiation-induced unrepaired DSBs by anti-pCHD7 antibody staining. (A) Structure of the CHD7 protein and (B) potential site of ATM kinase–mediated phosphorylation. (C) pCHD7 and γH2AX antibody staining of 10 Gy-3 wk cultured cells. (D) Western blot analysis with anti-pCHD7, CHD7, and TBP antibody. TBP: TATA-binding protein as internal control. (E) Effect of ATM kinase inhibitor, KU55933, on the repair foci formation in cells at 1 Gy-1 h. pCHD7 staining appears red. (F) The effect of the polyubiquitination inhibitor MG132 on the repair foci formation in 1 Gy-1 h cells. Note that contrast was enhanced in some of the photo images, for example, in F, MG132 (+) 53BP1, to confirm the lack of positive signals in the very dark nuclear images. Scale bar, 5 μm.

(Figure 1C) (Noda *et al.*, 2015a). Such quiescent cells appeared to be alive and healthy (Figure 1D) in a prolonged culture.

To characterize the cells at the molecular level, total RNA was extracted from quiescent cultures of human diploid fibroblasts (HCA2) 1 mo after exposure to 10 Gy (abbreviated 10 Gy-1 Mo), in which all the cells carried several pairs of unrepaired DSBs, or 10 Gy-1.5 h or 0 Gy (control cultures; Figure 1E). Using comparative hybridization screening with the Agilent human gene expression array, we selected genes with expression that had remained relatively unchanged or had become down-regulated at 1.5 h and that had, subsequently, become specifically up-regulated at 10 Gy-1 Mo (log2 ratio >1). A total of 196 genes were ultimately selected, including hypothetical genes (Supplemental Data 1); however, further selection of genes coding for nuclear proteins and chromatin factors revealed 16 genes that might be unique to cells bearing unrepaired DSBs (Figure 1, D–F). These included *HSF5*, *TOP2A WDR65*, *TP63*, *ATM*, *MDM1*, and *FANCA*.

Phosphorylated ATM (pATM hereafter) remains at unrepaired DSBs with a turnover rate less than 1 d (Noda *et al.*, 2012). Thus, ATM signaling must become activated at the unrepaired DSB foci. As ATM signaling has wide-ranging implications through its kinase activity—ATM kinase may have as many as 700 potential target proteins (Matsuoka *et al.*, 2007)—each ATM downstream effector protein may exert unique biological roles. Subsequently, CHD7 was identified from searches for proteins containing the ATM kinase target serine-glutamine (SQ) sequence that were encoded by the above-mentioned 16 candidate genes.

Generation and validation of antibodies against phosphorylated CHD7

Considering that CHD7 contains a serine at position 2255 that can form the SQ sequence (Figure 2, A and B), it may represent an ATM target (Matsuoka *et al.*, 2007; Zentner *et al.*, 2010). Therefore, we created a rabbit polyclonal antibody against the s2255 phosphorylated form of CHD7 (hereafter, pCHD7). This antibody detected the localization of pCHD7 (stained red) in unrepaired DSBs, together with γH2AX (Figure 2C) long time after high-dose radiation exposure. These unrepaired DSB foci also included 53BP1 and polyubiquitin. Western blotting using the HCA2 cell nuclear lysate detected a specific band at an expected molecular size, further revealing that phosphorylation of CHD7 was initiated within 1 h following irradiation and continued for more than 1 mo unless the damage was repaired (Figure 2D).

Next, we assessed the ATM dependency of CHD7 phosphorylation. Because the formation of DSB foci by pCHD7 occurred rapidly and the pCHD7 foci colocalized with γH2AX foci (forming nearly 30 DSB foci 1 h post–1 Gy exposure), we assessed the foci formation at 1 Gy-1 h. Overnight pretreatment of cells with 10 μM KU55933, an inhibitor of ATM kinase, completely abolished ATM

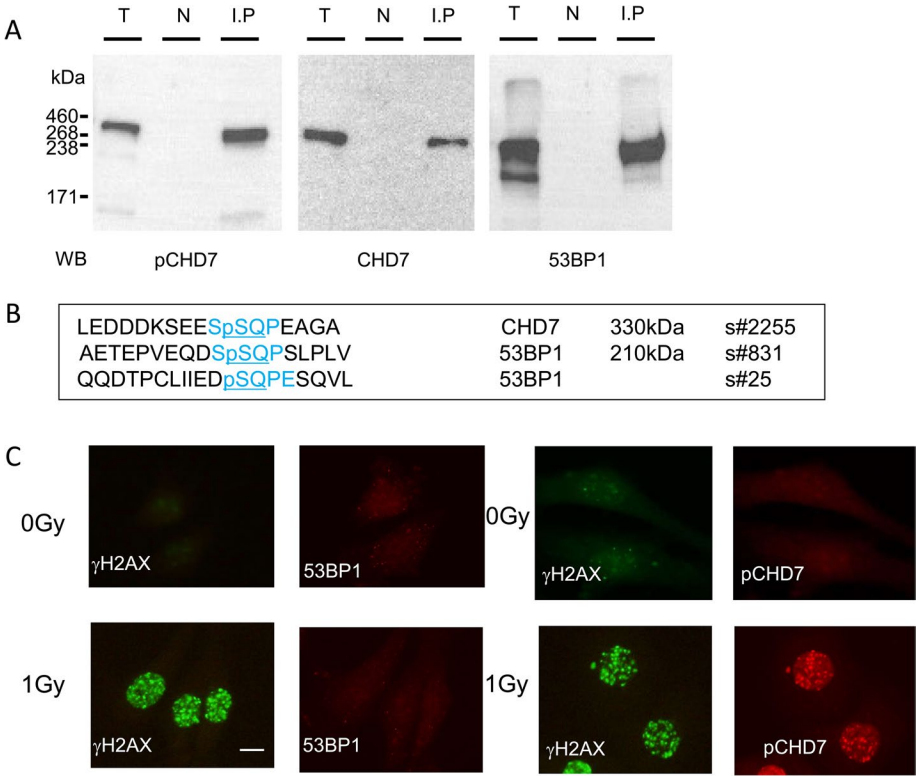

FIGURE 3: Characterization of pCHD7 antibody by immunoprecipitation and cell staining. (A) Cell lysates from 5 Gy-1 h HCA2 were subjected to immunoprecipitation using the pCHD7 antibody. Then, the samples were analyzed by Western blotting using pCHD7, CHD7, or 53BP1 antibodies. Individual lanes indicate: T, total nuclear proteins; N, normal goat IgG used for the control of immunoprecipitation; and I.P, a pCHD7 antibody was used for immunoprecipitation. (B) Four-aa SSQP sequence including ATM kinase target SQ at the serine 2255 in CHD7 also exists at serine 831 in 53BP1. Furthermore, the serine position of CHD7 also matches at the serine 25 in 53BP1, with one aa shifted to make the four-aa sequence SQPE. (C) pCHD7 foci formation at DSB sites following irradiation in *53BP1*-KO MEFs. Colocalization of pCHD7 and γH2AX was observed after irradiation (1 Gy in right panel) but no 53BP1 foci were observed (1 Gy in left panel). Scale bar, 5 μm.

self-phosphorylation and its accumulation in DSB sites after irradiation (Figure 2E). Additionally, γH2AX foci formation was significantly, although not completely, reduced. Meanwhile, in the control that was not treated with KU55933 (KU55933 [–]), DSB foci, containing pATM and pCHD7 were relatively similar to those observed with γH2AX and pCHD7 foci. In this setting, the formation and accumulation of pCHD7 was completely inhibited in KU55933 (+) cells (Figure 2E and Supplemental Figure 1).

Formation of DSB foci with γH2AX and 53BP1, as well as subsequent initiation and propagation of stress signals, requires polyubiquitination of the focus proteins (Kolas *et al.*, 2007; Noda *et al.*, 2012). Pretreating cells for 2 h with 5 μM MG132, an inhibitor of substrate polyubiquitination, completely inhibited 53BP1 and pCHD7 accumulation after irradiation, whereas the γH2AX foci were unaffected (Figure 2F), indicating that serine 2255 phosphorylation of CHD7 is ATM dependent and the process occurs downstream of γH2AX foci formation.

We next assessed possible interactions between pCHD7 and 53BP1 using coimmunoprecipitation and Western blot analyses (Figure 3A). Antibodies against pCHD7, CHD7 (nonphosphorylated form), and 53BP1 detected specific bands in an immunoprecipitate with the anti-pCHD7 antibody. However, the 53BP1 protein band appeared to overlap with pCHD7 and was indistinguishable even in normal or gradient SDS–PAGE analyses. Because the kinetics of foci formation by pCHD7 and 53BP1 remained the same (Figure 2F), we suspected that our pCHD7-specific antibody cross-reacted with 53BP1. That is, although the calculated molecular weight differed somewhat, the protein behaviors in the gel were similar. In fact, a four-amino-acid (aa) sequence in the CHD7 epitope, the SSQP sequence, was also detected in human 53BP1 at serine 831 (Figure 3B; S831 in human 53BP1). Moreover, the SQPE sequence at the same location in CHD7 was also observed in human 53BP1 at serine 25. Hence the human CHD7 serine 2255 site, which formed an SQ sequence for ATM targeting, matches human 53BP1 with two four-aa sequences. In mouse 53BP1, only the SQPE sequence is conserved at serine 30. Therefore, our anti-pCHD7 antibody may cross-react with phosphorylated forms of 53BP1 if the four-aa sequence including SQ has sufficient antigenicity. To address this issue, we created a FLAG-tagged *CHD7* cDNA plasmid construct, which was used to transfect HeLa cells. Immunoprecipitation with the anti-FLAG antibody strongly reacted with pCHD7 and CHD7 antibodies but scarcely with the 53BP1 antibody (Supplemental Figure 2B), suggesting phosphorylation of exogeneous FLAG-CHD7 following irradiation. In contrast, when the FLAG-*53BP1* construct was transfected, immunoprecipitation with an anti-FLAG antibody revealed that the precipitate strongly reacted with the anti-pCHD7 antibody (Supplemental Figure 2C, right panel). This might be caused by binding of the pCHD7 antibody with phosphorylated FLAG-53BP1 or coimmunoprecipitation of FLAG-53BP1 and pCHD7. Meanwhile, 53BP1 was not detected in the immunoprecipitate with a CHD7 (nonphosphorylated) antibody (Supplemental Figure 2D), and the anti-CHD7 antibody failed to detect CHD7 in the immunoprecipitate from FLAG-*53BP1*–transfected cell lysate using an anti-FLAG antibody (Supplemental Figure 2E). Hence, we concluded that the generated antibody against pCHD7 cross-reacts with the phosphorylated form of 53BP1. However, considering that Western blot analyses did not reveal any other bands, we postulate that no other cross-reactivity occurred. With anti-FLAG antibody staining, we confirmed that exogenously introduced FLAG-CHD7 was phosphorylated (Supplemental Figure 2B) and accumulated to form DSB foci after irradiation (Supplemental Figure 2F), further demonstrating DSB foci formation of phosphorylated CHD7 protein irrespective of the antibody specificity.

Anti-pCHD7 antibodies were generated twice ($n = 4$ total); all of them exhibited comparably strong reactivities. Furthermore, to improve antibody specificity, we made slight alterations to the antigen epitope sequence, from KSEESpSQPEAG to DDDKSEESpSQ; however, another two rabbits immunized with the latter sequence also produced antibodies with the same potency and specificity. The aa sequence DDDKSEESSQPEAGA (Figure 2B), which includes the targeted SQ, is completely conserved among many species, including mouse, rat, chicken, cow, elephant, and chimpanzee.

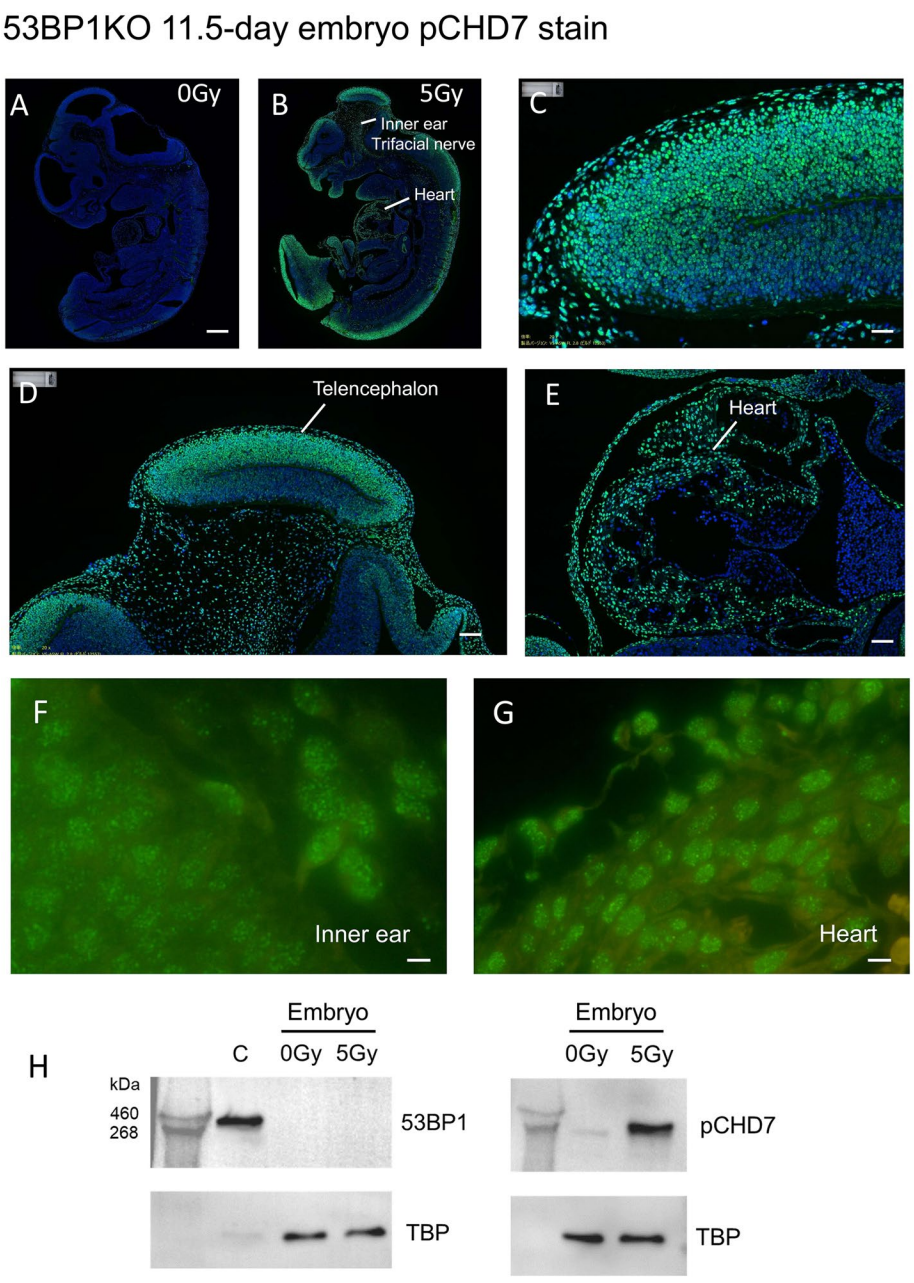

FIGURE 4: pCHD7 immunostaining in an 11.5-d-old *53BP1*-KO embryo 1 h post a 5-Gy exposure. pCHD7 staining showed green color, and DAPI showed blue. (A) 0 Gy control, scale bar, 500 μm; (B–E) pCHD7 staining 1 h after 5 Gy exposure: (B) whole embryo; (C) the front of the head, scale bar, 30 μm; (D) head; (E) enlarged view of the heart, scale bar 150 μm. (F, G) Enlarged view of inner ear and heart, scale bar 20 μm. (H) Western analyses of whole embryo lysate.

Accumulation of pCHD7 at DSB foci in a 53BP1-null background

As the anti-pCHD7 antibody has been suggested to cross-react with the phosphorylated form of 53BP1, we assessed the radiation response of CHD7 in a 53BP1-null background (Ward *et al.*, 2003). The results confirmed pCHD7 accumulation in DSB foci (Figure 3C). The cells used were MEFs derived from a 53BP1-KO mouse embryo, and 53BP1 expression was not detected. These results confirmed that CHD7 is phosphorylated upon radiation exposure and accumulates in DSB foci.

CHD7 expressed in tissues derived from neural crest cells forms DSB foci after radiation exposure in an 11.5-d-old mouse embryo

Considering that the morphogenesis of neural crest–derived tissue peaks on day 11.5 of the embryo, wild-type (WT) (C57BL) mouse embryos aged 11.5 d were collected from the uterus, irradiated at 5 Gy, and incubated in culture media for 1 h. Whole embryo sections were prepared and stained with pCHD7 antibody. The antibody strongly reacted with the developing organs (Supplemental Figure 3, 5 Gy), which was not observed in unirradiated littermate embryos (Supplemental Figure 3, 0 Gy). In particular, the developing heart, inner ear, trifacial nerve, telencephalon, and eyes exhibited strong staining (Supplemental Figure 3, D–F), and typical DSB foci were observed (Supplemental Figure 3, G and H, enlarged views).

Next, we performed the same experiment in *53BP1*-KO mouse embryos and obtained similar results: pCHD7-positive cells were clearly observed during the morphogenesis stage of the telencephalon, eyes, and heart after radiation exposure (Figure 4, A–G). Background staining of pCHD7 was much lower in 53BP1-null embryos and was not observed in the 0 Gy controls. Western blot analyses of whole embryo extracts further confirmed CHD7 phosphorylation upon irradiation in a 53BP1-null background (Figure 4H). Given that pCHD7 foci formed in a 53BP1-null background (Figure 4, F and G) and that Western blot analyses did not reveal any extra bands, we concluded that CHD7 becomes phosphorylated and accumulates at DSB sites following radiation exposure in certain developing organs.

Upon phosphorylation, CHD7 loses enhancer binding activity and moves to DSB sites

Next, we used a typical CHD7-binding sequence, the HS2 enhancer of the locus control region (LCR) of the globin gene promoter (Schnetz *et al.*, 2009), and assessed CHD7-binding activity after radiation in cultured DLD-1 cells. More specifically, chromatin immunoprecipitation (ChIP) was employed to evaluate CHD7-binding activity to the LCR, revealing that this binding activity rapidly decreased following irradiation (Figure 5A), while the binding of histone H3K4Me3, a marker of active chromatin, did not exhibit marked changes or showed a gradual decline (Figure 5B). Moreover, pretreatment of cells with KU55933 significantly protected them from the radiation-induced decrease in CHD7 binding to the LCR (HS2) sequence, suggesting that this decline was attributable to the phosphorylation of CHD7 by ATM (Figure 5C). However, no such effect was observed in H3K4Me3 binding to LCR.

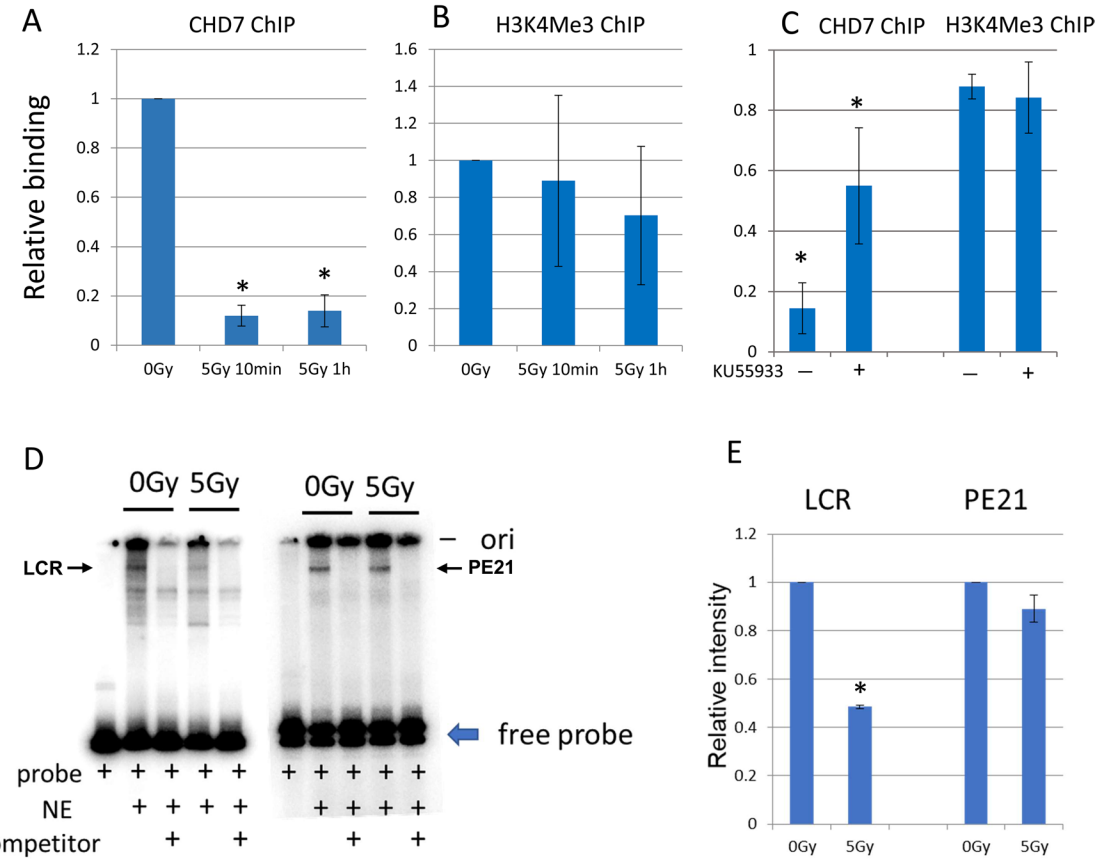

FIGURE 5: Release of CHD7 proteins from the LCR HS2 sequence in the globin gene after radiation exposure. (A–C) ChIP assay. (A) Relative amount of CHD7 bound to LCR (HS2) sequence. (B) Relative amount of histone H3K4Me3 bound to LCR (HS2) sequence. (C) Relative amount of CHD7 or H3K4Me3 bound to LCR (HS2) 10 min after exposure at 5 Gy in cells with or without KU55933 pretreatment. The data are the average of four experiments with SD, *t* test, $*p < 10^{-4}$. (D, E) Gel mobility shift assay of LCR sequence; in D the arrow in the left panel indicates the decrease of the LCR shifted band following irradiation. The arrow in the right panel indicates no change in the PE21 shifted band after irradiation in the control. Probe, radiolabeled LCR or PE21; NE, nuclear extract; competitor, excess amount of nonradiolabeled LCR or PE21. (E) Relative amount of nuclear protein binding to LCR or PE21. The data are the average of two experiments with SD; * $p < 0.01$.

Next, a radiolabeled LCR probe was used for gel mobility shift analysis to monitor LCR binding proteins, revealing a reduction following radiation exposure (Figure 5, D and E, left panel). The specificity of the shifted bands was confirmed via the addition of excess unlabeled probes (10×) as competitors. The control PE21 probe is a transcriptional element in the p53 promoter that does not respond to ionizing radiation exposure (Figure 5, D and E, right panel) (Noda *et al.*, 2000). As in previous experiments, KU55933 pretreatment suppressed the reduction in shifted bands following radiation (Supplemental Figure 4A; compare lanes 4 and 8 in B). These results further suggest that CHD7 is phosphorylated following radiation exposure, after which it translocates from the promoter/enhancer to DBS sites.

In vitro *CHD7* knockout causes moderate radiation sensitivity and cells exhibit unexpected response following additional *53BP1* knockout

To determine the role of CHD7 in the radiation-stress response, we first examined the effect of *CHD7* knockdown (KD). In HeLa cells, KD induced radiation sensitivity, depending on the degree of decreased CHD7 expression (Supplemental Figure 5). Next, we created *CHD7*-knockout (KO) cells using HT1080 cells carrying a stable diploid karyotype. For comparison, *53BP1*-KO and *CHD7/53BP1*-double KO (DKO) cells were also created (Supplemental Figure 6). The growth rate of *CHD7*-KO HT1080 cells was comparable to that of parental WT cells and became moderately radiation sensitive (10% sensitization when evaluated with D_{37}: 37% survival dose) (Figure 6, A and B). In contrast, *53BP1*-KO cells exhibited apparent growth retardation (12% lower growth rate), with a considerable increase in radiation sensitivity (40% sensitization at D_{37}). In DKO cells the growth rate was further decreased by 24%; that is, the doubling time extended from 29.5 h in WT to 38.6 h in DKO cells. However, the radiation sensitivity of DKO cells was reversed, with them becoming more resistant than the *53BP1*-KO cells. In fact, they seemed to be comparable to *CHD7*-KO cells, indicating that the CHD7 defect helped the *53BP1*-KO cells survive (Figure 6, B and C).

Loss of CHD7 induces error-prone nonhomologous end joining

Although we confirmed that CHD7 is phosphorylated and accumulates in DSB foci, it remained uncertain whether the protein directly participates in the DSB repair process as cells lacking CHD7 did not exhibit high sensitivity to radiation. Therefore, we evaluated the effect of CHD7 deficiency on nonhomologous end joining (NHEJ) activity. To this end we utilized the green fluorescent protein (GFP) reporter system, in which the occurrence of NHEJ can be monitored in cells integrated with the plasmid pEJ via transient introduction of

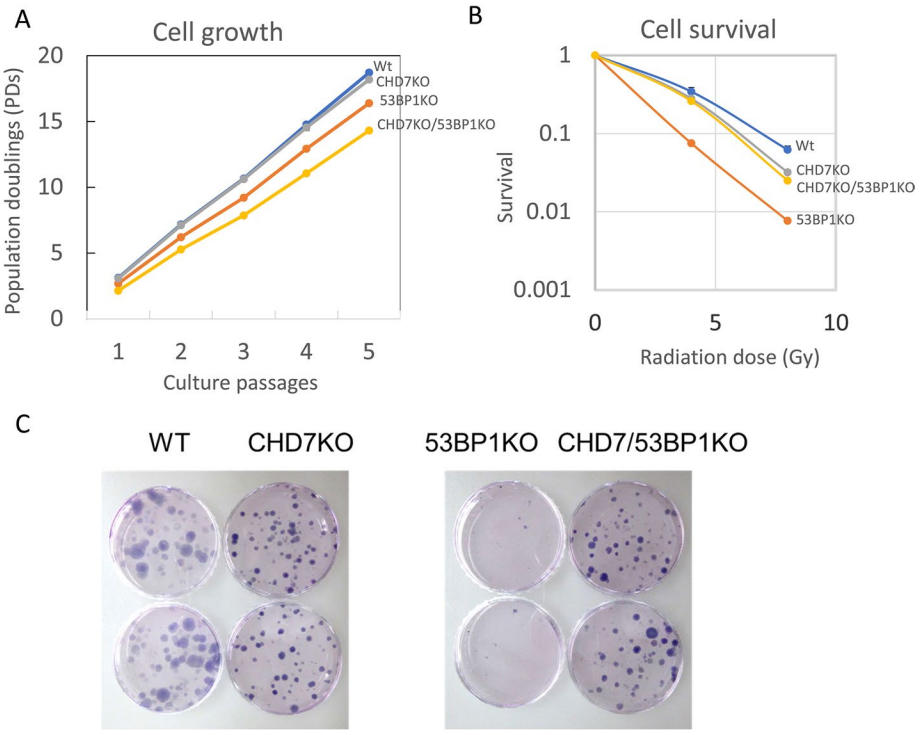

FIGURE 6: Targeted disruption of *CHD7* and/or *53BP1* changes cell growth and radiation sensitivity. (A) Growth curve of each cell strain in comparison with WT HT1080. (B) Cell survival following radiation exposure. (C) Colony formation of each cell strain; 1600 cells of each strain were inoculated in duplicate dishes, and after 8 Gy x-ray irradiation, cells were cultured for 12 d to fix and stain. The data are shown as average with SD.

DSBs (Mansour *et al.*, 2010) at two predetermined adjacent positions, where the DSBs produce noncompatible (noncohesive) overhangs (Supplemental Figure 7). In *CHD7*-KO cells, the system produced an increased number of GFP-positive cells, indicating enhanced NHEJ (Figure 7, A–C). Sequencing of the junction at the DSB rejoining portion in GFP(+) cells revealed an increase in deletion size in *CHD7*-KO cells (Figure 7D; Supplemental Figure 8). In fact, WT HT1080 cells showed 0.04–2.5 base deletions on average in two independent clones, respectively (indicating typical NHEJ) at the DSB sites, *CHD7*-KO cells had an average deletion size of 20.3–37.0 bases. Furthermore, we often observed cell clones with >100 base pair deletions at DSB sites, which was not seen in WT cells. Therefore, it is noted that *CHD7*-KO cells have a potential for producing both small (typical NHEJ) and larger deletions (nontypical NHEJ); the latter tends to increase. When defining typical NHEJ as Indel production within 1–5 bases, large deletions (>5 base pairs) were significantly more prevalent in *CHD7*-KO cells compared with Parental, *53BP1*-KO, and DKO cell lines (all $p < 0.001$).

In contrast, *53BP1*-KO cells did not exhibit an increase in the average deletion size (1.2–5.0 base deletion) at DSB sites, indicating that *53BP1*-KO increased the NHEJ frequency (Figure 7C); however, the actual deletion size remained small. Meanwhile, the NHEJ frequency was significantly reduced in DKO cells, and the deletion size in GFP(+) cells was not significantly increased (average 4.2–5.9). There was no evidence of a large difference in prevalence in Parental versus *53BP1*-KO ($p = 0.70$), Parental versus DKO ($p = 0.87$), or *53BP1* versus DKO ($p = 0.88$). In many cases, processing of the noncompatible overhangs led to simple fill-in of one additional "A" as in WT cells (Supplemental Figure 8), which was originally reported by Mansour *et al.* (2010).

We also performed a conventional mutation assay using the *HPRT* gene locus located on the X chromosome, where the loss of the gene activity by mutation can be detected as 6TG resistance of cells. The results confirmed an increase in radiation-induced mutations in *CHD7*-KO cells (Figure 7E). Radiation-induced mutation was also increased in *53BP1*-KO cells; however, the dose response appeared to be somewhat complicated, as it did not seem to be dose dependent. That is, the response was lower at 6 Gy than at 3 Gy. This may have been due to the high radiation toxicity to *53BP1*-KO cells. In contrast, *CHD7/53BP1*-DKO cells exhibited relatively no increase in NHEJ events (Figure 7C), even in *HPRT* locus mutations after radiation exposure (Figure 7E). The DKO cells exhibited a very low background and scarcely detectable spontaneous mutation frequencies.

DISCUSSION

In search of proteins that are expressed in cells bearing unrepaired DSBs, we identified ATM-dependent phosphorylation of CHD7 at DSB sites, which remained as long as the damage persisted. Furthermore, most major players in DSB foci, such as γH2AX, 53BP1, MDC1, Rap80, and polyUb, along with pCHD7, remained at unrepaired DSBs, indicating that repair signaling remains activated until the damage is removed from the genome (Noda *et al.*, 2012). Recently, Rother *et al.* (2020) reported the localization of CHD7 at DSBs in U2OS cells, while Ahmed *et al.* (2021) also reported the role of CHD7 in oxygen radical stress in mouse auditory and sensory hair neurons. In line with these studies, we report, for the first time, the participation of CHD7 in the DSB repair process via ATM signaling in early development. Hence, CHD7 belongs to the ATM-mediated chromatin repair network.

To the best of our knowledge, commercially available CHD7 pan-antibodies, including those manufactured by Cell Signaling, Abcam, and Novus Bio, do not efficiently detect radiation-induced DSBs unless the nuclei are substantially damaged, and the use of an UV laser in combination with bromodeoxyuridine (BrdU) prelabeling is required (Rother *et al.*, 2020). In contrast, our antibody against pCHD7 is able to detect a single DSB. As such, this antibody revealed a new role for CHD7 as a transcription factor indispensable for neural crest cell differentiation and genome damage response. We propose a "morphogenesis-coupled repair" in vertebrate embryogenesis, for which S2255 phosphorylation acts as a functional switch.

CHD7 induces neural crest cells to differentiate into neurosensory organs and to build craniofacial and heart architecture (Layman *et al.*, 2010; Schulz *et al.*, 2014; Feng *et al.*, 2017; Whittaker *et al.*, 2017; Yan *et al.*, 2020). Given the developmental link between the head and the heart (Maxmen, 2022), the role of CHD7 is intriguing, as it controls the morphogenesis of these organs through the small cell population. Although CHD7 is ubiquitously expressed, its expression increases during certain stages of development and is indispensable for cerebellar development (E12.5–14.5) (Feng *et al.*, 2017).

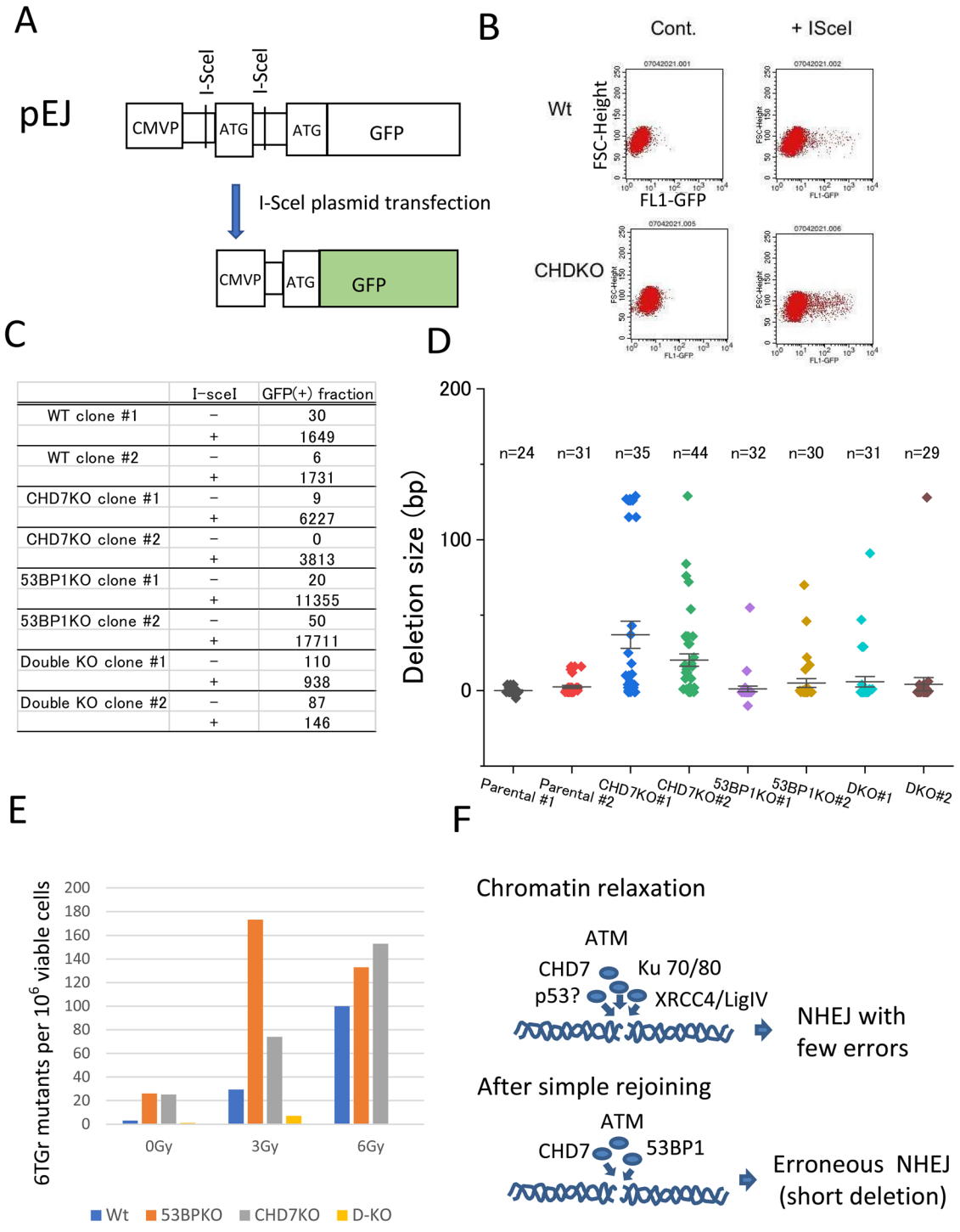

	I-sceI	GFP(+) fraction
WT clone #1	−	30
	+	1649
WT clone #2	−	6
	+	1731
CHD7KO clone #1	−	9
	+	6227
CHD7KO clone #2	−	0
	+	3813
53BP1KO clone #1	−	20
	+	11355
53BP1KO clone #2	−	50
	+	17711
Double KO clone #1	−	110
	+	938
Double KO clone #2	−	87
	+	146

FIGURE 7: Loss of *CHD7* induces error-prone NHEJ and mutations. (A) Structure of the NHEJ reporter plasmid pEJ. (B) Flow cytometric detection of I-SceI–induced GFP-positive cells. (C) Number of GFP-positive cells in 10^6 cells with or without pCBASceI transfection. Two independent clones, each from WT and KO cells, are shown. (D) Size distribution of deletions occurring at DSB sites. The data are shown as the average sizes of deletions in GFP-positive cells with SE: Parental #1, 0.04 ± 0.4; Parental #2, 2.5 ± 1.1; CHD7KO #1, 37.0 ± 5.9; CHD7KO #2, 20.3 ± 4.1; 53BP1KO #1, 1.2 ± 1.8; 53BP1KO #2, 5.0 ± 2.9; DKO #1, 5.9 ± 3.5; DKO #2, 4.2 ± 4.4. (E) Frequency of *HPRT* mutations in 10^6 viable cells after radiation. (F) Model depicting CHD7 involvement in DSB foci complex under the ATM control.

How does such an important transcription factor respond to genome stress? Our data indicate that following irradiation, CHD7 is phosphorylated and moves to the DSB sites. This phenomenon implies that during the "point of no return" biological process, CHD7 has two key functions: progression of development and DNA damage response. However, as the timeline is strictly predetermined in early development, priority cannot be given to either. Therefore, the cells must effectively repair the damage and fulfill morphogenesis within the scheduled time. If the damage is too extensive, the available number of transcription factors may become temporarily

reduced, resulting in a condition similar to CHARGE, by decreasing the number of differentiated cells or attaining imperfect morphogenesis. This is a plausible cause of radiation-induced malformations in neonates. In this context, our finding that CHD7 phosphorylation is strongly induced in the fetal brain and heart after irradiation (Figure 4, D and E, and Supplemental Figure 3) is significant.

Nevertheless, we still have no direct evidence of the involvement of pCHD7 in DSB repair. CHD7 ablation in HT1080 cells resulted in only modest radiation sensitization. However, this improved the survival of 53BP1-deficient cells. Our results suggest a mechanism by which CHD7 facilitates less error-prone (smaller deletion size) NHEJ and show that canonical NHEJ is possible with CHD7, in the absence of 53BP1. CHD7 has been proposed to relax chromatin to promote error-free NHEJ (via Ku and ligase) before 53BP1 activation (Rother *et al.*, 2020), in which the 53BP1 signal handles the remaining DSBs through erroneous NHEJ (Figure 7F). Our data confirmed increased deletion size at DSB sites in CHD7-deficient HT1080 cells. In contrast, NHEJ activity of *CHD7/53BP1*-DKO cells was comparable in WT cells or slightly reduced, resulting in a somewhat hypomutable phenotype. Similarly, radiation-induced *HPRT* gene mutations were extensively suppressed. Moreover, spontaneous mutations at the *HPRT* locus rarely occurred. This may indicate that, in *CHD7/53BP1*-DKO HT1080, most DSBs are repaired error-free via the homologous recombination repair system in a subsequent DNA replication. However, this might be specific to HT1080 cells, which divide indefinitely. Cells at the embryonic developmental stage may not be capable of altering the repair system so readily, resulting in cell death. Apart from immortalized HT1080 cells, CHD7 expression in the neural crest cells of embryos was quite high. Assuming that such cells in the developing embryo are much more radiation sensitive, the CHARGE syndrome phenotype, which includes frequent malformation of the heart and neurosensory organs, can be easily explained.

Developing embryos exhibit high radiation sensitivity. In experimental animals, embryos are most sensitive during the morphogenetic stage (Rugh and Wohlfromm, 1965; Hall, 1994; ICRP, 2003). The p53 protein, as a guardian of the genome, suppresses malformation by inducing apoptosis in damaged cells (Norimura *et al.*, 1996; Nomoto *et al.*, 1998). In contrast, CHD7 may suppress embryonal death and malformation through the DNA damage response, likely by promoting DSB repair. In both systems, excessive damage may cause the embryo to either die or survive with morphological failure. In that sense, CHD7 and p53 are the two sides of the same coin, as positive or negative regulators. Indeed, inappropriate activation of p53 in developing embryos causes CHARGE-like symptoms by producing multiple deformities (Van Nostrand *et al.*, 2014). Moreover, Wang *et al.* (2022) recently demonstrated that p53 promptly (within seconds) binds to damaged sites through its C-terminal polyadenylation and promotes error-free NHEJ. Thus, CHD7 and p53 may also cooperate, or compete, during the very early stage of the damage response, for chromatin relaxation, not through their transcriptional activities (Figure 7F). While Rother *et al.* (2020) proposed PARP-triggered accumulation of CHD7, they did not elucidate the role of ATM; however, our results clearly show ATM-dependent phosphorylation at DSBs. Meanwhile, Wang *et al.* (2022) suggested an initial role of p53 PARylation, but not CHD7, in chromatin relaxation at DSBs. Further analysis will provide clearer insights into the role of these proteins in chromatin relaxation.

The effects of fetal radiation exposure have been investigated in humans. For instance, in utero exposure of atomic bomb survivors in Hiroshima and Nagasaki resulted in cranial nerve system abnormalities during the second stage of gestation (8–15 wk), with dose-dependent increases in mental illness and microcephaly (Otake *et al.*, 1991; Otake and Schull, 1998; Hall, 1994). Our results provide novel insights into the role of CHD7 in radiation stress and cranial nerve system development.

Our findings may be further generalized by including development- and differentiation-related transcription factors. More specifically, the key transcription factors that control development may have a direct or indirect function in the genome stress response. There are three such examples: 1) Pax2 transcription factor–interacting protein 1 (PTIP1) physically interacts with Pax2, a key protein in kidney morphogenesis (Dahl *et al.*, 1997). Neonates born following *PAX2*-KO lack kidneys (Torres *et al.*, 1995). PTIP1 was subsequently found to serve as a typical DSB foci protein after radiation exposure (Gong *et al.*, 2009; Muñoz and Rouse, 2009; Callen *et al.*, 2020). 2) Cofactor of BRCA1 (COBRA1), which controls mammary gland development, is physically associated with BRCA1, suggesting that the BRCA1/COBRA1 complex regulates DSB repair and mammary gland morphogenesis (Nair *et al.*, 2016). 3) BRCT-repeat inhibitor of hTERT expression 1 (BRIT1), also known as microcephalin 1 (MCPH1), is a transcription factor that suppresses hTERT expression in differentiated cells and is responsible for microcephaly; however, it is also a typical DSB foci protein that responds to radiation (Lin *et al.*, 2005).

Taking the data together, we propose that vertebrates have evolved a morphogenesis-coupled genome stress response in early embryogenesis. The central mechanisms involved in maintaining the continuity of life consist of DNA replication/transcription and cell division/ontogenesis. As DNA replication has proofreading mechanisms, and for transcription, the mechanism itself includes a transcription-coupled repair system, it is reasonable to suppose that morphogenesis-coupled repair is part of vertebrate embryogenesis. Future studies will delineate the precise molecular mechanisms of how pCHD7 modulates the activity of the DSB repair protein complex during embryonal morphogenesis stages to ensure genome integrity and progression of normal development.

MATERIALS AND METHODS

Request a protocol through *Bio-protocol*.

Cell lines and culture

HCA2, a normal human diploid fibroblast cell line, also known as MJ90 (Noda *et al.*, 2012, 2015a), *53BP1*-KO MEFs, and tumor cell lines (HeLa S3, HT1080, and DLD-1, all purchased from the American Type Culture Collection) were cultured in 5% CO_2 at 37°C with EMEM (Earl's salts) supplemented with 10% fetal calf serum (FCS). *53BP1*-KO MEFs were a gift from David Chen of MD Anderson (Houston, TX) (Ward *et al.*, 2003). Human diploid fibroblasts were deemed suitable for observing unrepaired DSBs as they can create a stable G_o phase. Meanwhile, HeLa S3 and HT1080 were deemed suitable for IP and gene transfer, while HT1080 cells were particularly appropriate for creation of KO cells by gene editing. DLD-1 is a cell for which the CHD7-binding sequence has been reported, and data are available on LCR (H2 enhancer) binding (Schnetz *et al.*, 2009).

To observe unrepaired DSB foci, HCA2 cells were transferred to EMEM containing 0.1% FCS and cultured for more than 1 wk to become quiescent (G_o) cells. Such G_o cells can be maintained for more than 1 y in stable quiescence by weekly medium changes (Noda *et al.*, 2012). X-ray irradiation was carried out using these quiescent cells, and the cells were periodically stained to observe unrepaired DSB foci or harvested to extract total RNA. Cells that could not be maintained in 0.1% FCS (MEFs and tumor cells) were cultured with 10% FCS. For treatment with an ATM kinase inhibitor, cells were

treated with 10 μM KU55933 (Tocris, Bristol, UK; cat. 3544) overnight, and then 1 h after 1 Gy exposure, cells were fixed and stained with various antibodies. Inhibition of polyubiquitination was carried out by 2 h of pretreatment with 5 μM MG132 (Boston BioChem, Cambridge, MA; cat. I-130), and 1 h after 1 Gy exposure, cells were fixed and stained. SA-βGal staining was carried out with 6 Gy-1 Mo cells using the Senescent Cells Staining Kit (Sigma-Aldrich, St Louis, MO; cat. CS0031-1KT).

Cell growth rate and x-ray survival were determined by conventional methods. For the growth test, 10^5 cells were inoculated in 6-cm dishes, harvested every 4 d, and counted, and the number of population doublings was calculated. Then, 10^5 cells from the culture were again inoculated. This process was repeated to obtain the growth curve. To determine the cell survival rate, a predetermined number of cells were inoculated onto 6-cm dishes, x-ray irradiated at a dose rate of 1 Gy/min, cultured for approximately 12 d, and then fixed and stained to count the cell colonies. Figure 6C shows the colony formation in duplicated dishes, in which 1600 cells were inoculated in each dish, irradiated with 8 Gy, and cultured for 12 d.

C57BL/6J and *53bp1*-KO mice

C57BL/6J mice and BS6:129-Trp53bp1tm1Jc/J mice (stock no. 006495) (Ward *et al*., 2003) were purchased from Charles River Laboratories Japan and the Jackson Laboratory (Bar Harbor, ME), respectively. The Radiation Effects Research Foundation (RERF) Animal Care and Use Committee approved this research under animal study protocol A-04.

Creation of specific antibodies against phosphorylated CHD7

An oligopeptide sequence (KSEESpSQPEAG) containing phosphorylated serine at position 2255 of human CHD7 was synthesized and used to immunize two rabbits. Both animals showed a strong antibody titer at the initial immunization and could react with DSB foci. After the third immunization, the antiserum was affinity purified by a phosphorylated peptide column and then a nonphosphorylated peptide column was used to remove antibody fractions against the nonphosphorylated form of the same peptide sequence. The pCHD7 antibody against the peptide sequence that slightly shifted the antigen epitope (DDDKSEESpSQ) was also created in the same manner. This antibody showed comparable potency to detect DSB foci. Peptide synthesis, rabbit immunization, and antibody purification were performed by Scrum Co., Ltd. (Tokyo, Japan).

Expression array analysis

Quiescent (G_o) cultures of HCA2 cells were irradiated with 10 Gy and cultured for 1.5 h or 1 mo, and then total RNA was extracted with TRIzol (Ambion, Austin, TX). The Agilent Expression array (SurePrint G3), which screened relative levels of gene expression across the entire genome, was performed by Takara Co., Ltd. (Kyoto, Japan). By comparing the expression levels of the 0 Gy control, 10 Gy-1.5 h, and 10 Gy-1 Mo, genes with expression levels that were comparable, or reduced, at 10 Gy-1.5 h and then subsequently increased by more than twofold at 10 Gy-1 Mo were selected (Supplemental Data 1). Nuclear genes that were already known to be involved in chromatin regulation/nucleic acid metabolism were selected.

Immunofluorescence analysis

Immunocytochemistry was performed using conventional methods. Briefly, cells grown on a coverslip in a 35-mm culture dish were washed with phosphate-buffered saline (PBS), fixed with 3.7% formaldehyde/PBS for 10 min at room temperature (approximately 20°C), and then treated with 0.5% Triton X-100/PBS for 5 min on ice. After blocking the cells with 10% normal goat serum (Invitrogen, Waltham, MA; cat. 50-062Z) for 10 min at room temperature, the first antibody was applied for 30 min at 37°C. The cells were then washed, and secondary antibodies conjugated with fluorescent probes were added. The antibodies used were 53BP1 (Bethyl, Montgomery, TX; A300-272A), γH2AX (Millipore, Burlington, MA; JBW301), and pATM (CST, Danvers, MA; 4526), all of which were diluted 1000–2000×. The secondary antibodies used were TRITC goat anti-rabbit immunoglobulin G (IgG) (Jackson, West Grove, PA) and Alexa Fluor 488 goat anti-mouse or anti-rabbit IgG (Invitrogen). The pCHD7 antibody we created was also used at 1000–2000× dilution.

Immunoprecipitation and Western blot analyses

Nuclear protein crude extracts were prepared from 3×10^6 irradiated cells using the Active Motif Co-IP kit (cat. 54002), mixed with 1 μg of the anti-pCHD7 antibody, and then immunoprecipitated using protein G-Fe beads. The bead-binding fractions were lysed with 2× Laemmli sample buffer and subjected to SDS–PAGE Western blotting using anti-pCHD7 and anti-CHD7 (CST; cat. 6505) and the anti-53BP1 antibody as noted above, respectively.

In a separate experiment, nuclear extracts from irradiated cells were subjected to immunoprecipitation with the anti-CHD7 antibody, followed by Western blotting using pCHD7 and 53BP1 antibodies. In experiments with FLAG-CHD7 and FLAG-53BP1 transfection and FLAG antibody pull down, plasmid vector pCMV-(DYKDDDDK)-N (Clontech, Mountain View, CA; 635688) and full-length cDNAs of CHD7 and 53BP1 were used to construct expression plasmids; then, 4 μg of each plasmid was transfected into 5×10^5 HeLa S3 cells. Two days after x-ray irradiation, cells were lysed, mixed with 1 μg of the anti-FLAG antibody (Clontech 635691 or Sigma F1804), and then the bead-binding fractions were analyzed by Western blotting with anti-pCHD7, CHD7, and 53BP1 antibodies.

Mouse whole embryos

Mouse embryos (E11.5) carrying WT or *53bp1*KO backgrounds were collected from pregnant mice, 5 Gy irradiated in a culture medium, and incubated for 1 h. Whole embryos were fixed with 4% paraformaldehyde/PBS, paraffin embedded to create whole embryo sections, and used for immunohistochemistry. Embryo immunofluorescence imaging with pCHD7 and 53BP1 antibodies was conducted at the Biopathology Institute Co., Ltd. (Ohita), using an Olympus Virtual Slide VS120 system. In a separate experiment, the head regions of the embryos were lysed with 2× Laemmli sample buffer or Active Motif's lysis buffer and subjected to Western blotting. The 0 Gy controls were littermates. The original images of the whole embryo virtual slides presented in Figure 4 and the Supplemental Figures can also be viewed on the web using Olympus OlyVIA (Freeware, https://www.olympus-lifescience.com/en/downloads/detail-iframe/?0[downloads][id]=847253503, or https://olyvia.software.informer.com/).

Virtual slide images are provided at https://drive.google.com/drive/folders/1z0CySF4JYSMoim0ovvlU3pKtT6n5a95R?usp=share_link.

Note that the web images must be downloaded first and then unzipped to be visualized in OlyVIA.

CHD7-knockdown

The *CHD7* small interfering RNA expression vector was constructed using the pBAsi-hU6Pur plasmid (Takara; cat. 3224); stably integrated HeLa cell clones were isolated. The relative amounts of *CHD7*-KD and changes in cell radiosensitivity were compared.

Targeted disruption of *CHD7* and/or *53BP1*

HT1080 cells, human fibrosarcoma cells carrying a stable near-diploid karyotype, were used for CRISPR/Cas9-mediated KO of *CHD7* and/or *53BP1* genes. For effective KO of *CHD7*, a previously reported site (Feng *et al.*, 2017) was chosen. The targeted DNA sequence for sgRNA (single guide RNA) synthesis was CTTTCTAGAGAAACCAGTGC, which was introduced into the plasmid pGuide-it-ZsGreen (Takara; cat. 632601), and the plasmid construct was transfected into HT1080 cells. GFP-positive cells were selected by cell sorting and individually cloned to examine *CHD7* gene disruption. To enhance the targeted KO of the two alleles, we applied cotransfection using a knock-in vector carrying the neomycin resistance gene. The 230 base pairs of upstream (left arm) and 240 base pairs of downstream (right arm) sequences of the CRISPR/Cas9 target site (DSB site) were obtained using PCR amplification of HT1080 genome DNA. Their sequences were inserted into the pBSneo-loxP vector (Noda *et al.*, 2015b) so that the neomycin resistance gene was sandwiched between them. Accordingly, the neomycin resistance gene could be inserted into the DSB site to destroy *CHD7* function. The PCR primers (5′–3′) were GTATTAACTAAAGTGCTATT, TGCTGAGAGACACAAATAGG (left arm), and GAATGCTCAGCTAGTGAAGA, GGTTCCTTCGGGTCAAAAAA (right arm).

After cotransfection with the plasmids, several cell clones bearing *Chd7* null (–/–) were obtained. One of the clones, which had a neomycin resistance gene inserted at one DBS site, was used for further experiments; for another allele, the 19-base deletion from the DSB site was observed, resulting in null production of the CHD7 protein. *53BP1*-KO HT1080 cells were also created in the same manner. That is, we set the DNA sequence GAAGTTTCCCCTTCACAGAC for sgRNA synthesis at the human 53BP1 exon 17, which matched the target site for *53bp1*-KO mouse creation (Ward *et al.*, 2003). In addition, 240 base pair upstream and downstream sequences of the target site were PCR amplified and inserted into the pBSneo-loxP to create knock-in vectors. The primer sequences (5′–3′) were as follows: AAGAACAGATCCTAAATGTT, TCTACAATTGGCTCTTCAGT (left arm), and CCTCCAAGGCATCCAGCTTA, TCCTGTGATATTAAAATGTC (right arm).

After cotransfection of CRISPR/Cas9 and knock-in vector plasmids, GFP-positive cells were recovered, one of which was used for further experiments and had a neomycin resistance gene at the DSB and a single base insertion at another DSB allele (leading to frameshift), resulting in null production of 53BP1 protein. To create *CHD7/53BP1*-double KO cells, the Cre recombinase expression plasmid, pcD-Cre, was transiently transfected into *CHD7*-KO cells; subsequently, neomycin-sensitive clones were isolated. These cells were then subjected to further *53bp1*-KO, as described above.

ChIP

For the enhancer/promoter binding assay of CHD7, the HS2 sequence of the LCR in the β-globin gene enhancer (Schnetz *et al.*, 2009) was used. Within this, 220 base pairs of the HS2 core sequence, isolated via PCR of DLD-1 genomic DNA with the primers (5′–3′) CAAGCATGAGCAGTTCTGGC and TTGCCATCTGCCCTGTAAGC, was used as the binding probe. DLD-1 cells were irradiated with 5 Gy, incubated for 10 min or 1 h, and fixed with formaldehyde. The reaction was stopped via the addition of 1.5 M glycine. Subsequently, the cells were briefly sonicated. After the debris was removed, an anti-CHD7 antibody (CST; 6505S) was added and incubated overnight at 4°C. Immunoprecipitation was performed by mixing the Protein A/G-Fe (Millipore; 16-663) beads for 1 h at 4°C; subsequently, the bead-binding fraction was eluted with 1% SDS/0.1 M $NaHCO_3$. After heating at 65°C for 4 h, CHD7-bound DNA was recovered by treatment with proteinase K and phenol extraction. The samples were subjected to real-time PCR to measure the relative amount of LCR (HS2) binding. To examine the effect of KU55933 on LCR (HS2) sequence binding, the agent was added at 10 μM in the culture 1 d before irradiation. As a control, an anti-H3K4Me3 antibody (Abcam, Cambridge, UK; ab8580), a marker of active chromatin, was also used for LCR (HS2) binding.

Gel shift analysis

Gel mobility shift assays were performed as previously reported (Noda *et al.*, 2000). In brief, nuclear protein extracts were prepared from control 0 Gy- and 5 Gy-irradiated and 1 h-incubated cells. The HS2 core sequence described above was end labeled via α^{32}P-dATP incorporation with the Klenow polymerase. The radiolabeled probe (3×10^6 dpm/ng DNA) and 7 μg of nuclear extract were mixed and incubated at 30°C for 30 min and then run in a neutral gel. As a competitor to determine the specific band, a 10-fold excess of nonlabeled probe DNA was also added in a parallel experiment. For comparison, the PE21 DNA element, which controls *p53* expression, was also used for the gel shift. PE21 does not respond to x-ray exposure (Noda *et al.*, 2000).

Mutation assay

The DSB repair reporter assay (Mansour *et al.*, 2010) was conducted with HT1080 WT or *CHD7*-KO and/or *53bp1*-KO cells carrying a single copy integration of plasmid pEJ in their genome. Two micrograms of the pCBASceI plasmid, which carries the I-*Sce*I endonuclease gene, was transiently transfected into 4×10^5 cells inoculated on the dishes. After 2 d of culture, the number of GFP-positive cells was measured by flow cytometry as cells underwent DSB-mediated NHEJ. The GFP-positive cells were isolated by cell sorting and individually cloned, and base sequences including two I-*Sce*I recognition sites were PCR amplified using the primers (5′–3′) GCAAATGGGCGGTAGGCGTG and TCGGGGCATGGCGGACTTGAA, which were inserted into the PCR2-Topo vector (Invitrogen) to determine the junction sequence resulting from the canonical or noncanonical NHEJ. Plasmids pEJ and PCBASceI were kindly provided by Wael Mansour (Hamburg, Germany).

The frequency of radiation-induced *HPRT* gene mutations was measured as reported previously (Noda *et al.*, 2011). Briefly, 2×10^6 cells were x-ray irradiated and cultured for 4 d, and then the cells were trypsinized and counted, and 10–20 10-cm dishes each containing 2.5 μg/ml 6-TG (6-thioguanine) were inoculated with 10^5 cells. Two weeks after drug selection, cells carrying *HPRT*-inactivating mutations were counted as 6-TG–resistant colonies. In parallel, the x-ray survival rate was also determined in this experimental setting, and mutation frequencies were calculated per 10^6 viable cells.

Statistical analysis

Data variability is expressed as mean ± SD or SE. In ChIP and gel shift experiments, a two-tailed Student's *t* test was performed to compare the unirradiated and irradiated samples. In NHEJ assays, the difference in the number of large (>5 base pairs) deletions between pairs of cell clones was tested using a two-sided test of proportions.

ACKNOWLEDGMENTS

We thank Wael Mansour for plasmids pEJ and pCBASceI, David Chen for 53BP1-KO MEFs, Mika Yamaoka for GFP-positive cell sorting, Richard Sposto of the Radiation Effects Research Foundation (RERF) Department of Statistics for statistical advice, and Nori Nakamura for advice on the manuscript. The RERF, Hiroshima and Nagasaki, Japan, dedicated to atomic bomb survivors, is a public interest foundation funded by the Japanese Ministry of Health, Labour and Welfare (MHLW) and the U.S. Department of Energy (DOE). The views of the authors do not necessarily reflect those of the two governments. This study was based on RERF research protocol A4-09. A. N. was partially supported by MEXT Grant 20K12179.

REFERENCES

Ahmed M, Moon R, Prajapati RS, James E, Albert Basson M, Streit A (2021). The chromatin remodelling factor Chd7 protects auditory neurons and sensory hair cells from stress-induced degeneration. Commun Biol 4, 1260.

Bajpai R, Chen DA, Rada-Iglesias A, Zhang J, Xiong Y, Helms J, Chang CP, Zhao Y, Swigut T, Wysocka J (2010). CHD7 cooperates with PBAF to control multipotent neural crest formation. Nature 463, 958–962.

Basson MA, van Ravenswaaij-Arts C (2015). Functional insights into chromatin remodelling from studies on CHARGE syndrome. Trends Genet 31, 600–611.

Bosman EA, Penn AC, Ambrose JC, Kettleborough R, Stemple DL, Steel KP (2005). Multiple mutations in mouse Chd7 provide models for CHARGE syndrome. Hum Mol Genet 14, 3463–3476.

Callen E, Zong D, Wu W, Wong N, Stanlie A, Ishikawa M, Pavani R, Dumitrache LC, Byrun AK, Mendez-Dorantes C, *et al*. (2020). 53BP1 enforces distinct pre- and post-resection blocks on homologous recombination. Mol Cell 77, 26–38.

Dahl E, Koseki H, Balling R (1997). Pax genes and organogenesis. BioEssays 19, 755–765.

Engelen E, Akinci U, Bryne JC, Hou J, Gontan C, Moen M, Szumska D, Kockx C, van Ijcken W, Dekkers DH, *et al*. (2011). Sox2 cooperates with Chd7 to regulate genes that are mutated in human syndromes. Nat Genet 43, 607–611.

Fan T, Huang Y (2021). Accessible chromatin reveals regulatory mechanisms underlying cell fate decisions during early embryogenesis. Sci Rep 11, 7896.

Feng W, Kawauchi D, Körkel-Qu H, Deng H, Serger E, Sieber L, Lieberman JA, Jimeno-González S, Lambo S, Hanna BS, *et al*. (2017). Chd7 is indispensable for mammalian brain development through activation of a neuronal differentiation programme. Nat Commun 8, 14758.

Gong Z, Cho YW, Kim JE, Ge K, Chen J (2009). Accumulation of Pax2 transactivation domain interaction protein (PTIP) at sites of DNA breaks via RNF8-dependent pathway is required for cell survival after DNA damage. J Biol Chem 284, 7284–7293.

Hall EJ (1994). Radiobiology for the Radiobiologist, 4th ed., Philadelphia, PA: J. B. Lippincott & Co.

He P, Williams BA, Trout D, Marinov GK, Amrhein H, Berghella L, Goh ST, Plajzer-Frick I, Afzal V, Pennacchio LA, *et al*. (2020). The changing mouse embryo transcriptome at whole tissue and single-cell resolution. Nature 583, 760–767.

Hurd EA, Capers PL, Blauwkamp MN, Adams ME, Raphael Y, Poucher HK, Martin DM (2007). Loss of Chd7 function in gene-trapped reporter mice is embryonic lethal and associated with severe defects in multiple developing tissues. Mamm Genome 18, 94–104.

ICRP (2003). Biological effects after prenatal irradiation (embryo and fetus). Ann ICRP 33, Publication 90.

Kolas NK, Chapman JR, Nakada S, Ylanko J, Chahwan R, Sweeney FD, Panier S, Mendez M, Wildenhain J, Thomson TM, *et al*. (2007). Orchestration of the DNA-damage response by the RNF8 ubiquitin ligase. Science 318, 1637–1640.

Layman WS, Hurd EA, Martin DM (2010). Chromodomain proteins in development: lessons from CHARGE syndrome. Clin Genet 78, 11–20.

Layman WS, McEwen DP, Beyer LA, Lalani SR, Fernbach SD, Oh E, Swaroop A, Hegg CC, Raphael Y, Martens JR, *et al*. (2009). Defects in neural stem cell proliferation and olfaction in Chd7 deficient mice indicate a mechanism for hyposmia in human CHARGE syndrome. Hum Mol Genet 18, 1909–1923.

Lin SY, Rai R, Li K, Xu ZX, Elledge SJ (2005). BRIT1/MCPH1 is a DNA damage responsive protein that regulates the BRCA1-Chk1 pathway, implicating checkpoint dysfunction in microcephaly. Proc Natl Acad Sci USA 102, 15105–15109.

Liu Y, Harmelink C, Peng Y, Chen Y, Wang Q, Jiao K (2014). CHD7 interacts with BMP R-SMADs to epigenetically regulate cardiogenesis in mice. Hum Mol Genet 23, 2145–2156.

Mansour WY, Rhein T, Dahm-Daphi J (2010). The alternative end-joining pathway for repair of DNA double-strand breaks requires PARP1 but is not dependent upon microhomologies. Nucleic Acids Res 38, 6065–6077.

Martin DM (2010). Chromatin remodeling in development and disease: focus on CHD7. PLoS Genet 6, e1001010.

Matsuoka S, Ballif BA, Smogorzewska A, McDonald ER 3rd, Hurov KE, Luo J, Bakalarski CE, Zhao Z, Solimini N, Lerenthal Y, *et al*. (2007). ATM and ATR substrate analysis reveals extensive protein networks responsive to DNA damage. Science 316, 1160–1166.

Maxmen A (2022). An ancient link between heart and head—as seen in the blobby, headless sea squirt. Nature. https://www.nature.com/articles/d41586-022-00413-y

Muñoz IM, Rouse J (2009). Control of histone methylation and genome stability by PTIP. EMBO Rep 10, 239–245.

Nair SJ, Zhang X, Chiang HC, Jahid MJ, Wang Y, Garza P, April C, Salathia N, Banerjee T, Alenazi FS, *et al*. (2016). Genetic suppression reveals DNA repair-independent antagonism between BRCA1 and COBRA1 in mammary gland development. Nat Commun 7, 10913.

Noda A (2018). Radiation-induced unrepairable DSBs: their role in the late effects of radiation and possible applications to biodosimetry. J Radiat Res 59, ii114–ii120.

Noda A, Hirai Y, Hamasaki K, Mitani H, Nakamura N, Kodama Y (2012). Unrepairable DNA double-strand breaks that are generated by ionising radiation determine the fate of normal human cells. J Cell Sci 125, 5280–5287.

Noda A, Hirai Y, Kodama Y, Kretzschmar WW, Hamasaki K, Kusunoki Y, Mitani H, Cullings HM, Nakamura N (2011). Easy detection of GFP-positive mutants following forward mutations at specific gene locus in cultured human cells. Mutat Res 721, 101–107.

Noda A, Mishima S, Hirai Y, Hamasaki K, Landes RD, Mitani H, Haga K, Kiyono T, Nakamura N, Kodama Y (2015a). Progerin, the protein responsible for the Hutchinson–Gilford progeria syndrome, increases the unrepaired DNA damages following exposure to ionizing radiation. Genes Environ 37, 13.

Noda A, Suemori H, Hirai Y, Hamasaki K, Kodama Y, Mitani H, Landes RD, Nakamura N (2015b). Creation of mice bearing a partial duplication of HPRT gene marked with a GFP gene and detection of revertant cells in situ as GFP-positive somatic cells. PLoS One 10, e0136041.

Noda A, Toma-Aiba Y, Fujiwara Y (2000). A unique, short sequence determines p53 gene basal and UV-inducible expression in normal human cells. Oncogene 19, 21–31.

Nomoto S, Ootsuyama A, Shioyama Y, Katsuki M, Kondo S, Norimura T (1998). The high susceptibility of heterozygous p53(+/–) mice to malformation after foetal irradiation is related to sub-competent apoptosis. Int J Radiat Biol 74, 419–429.

Norimura T, Nomoto S, Katsuki M, Gondo Y, Kondo S (1996). p53-dependent apoptosis suppresses radiation-induced teratogenesis. Nat Med 2, 577–580.

Otake M, Schull WJ (1998). Radiation-related brain damage and growth retardation among the prenatally exposed atomic bomb survivors. Int J Radiat Biol 74, 159–171.

Otake M, Schull WJ, Yoshimaru H (1991). A review of forty-five years study of Hiroshima and Nagasaki atomic bomb survivors. Brain damage among the prenatally exposed. J Radiat Res 32, 249–264.

Pauli S, Bajpai R, Borchers A (2017). CHARGEd with neural crest defects. Am J Med Genet C Semin Med Genet 175, 478–486.

Payne S, Burney MJ, McCue K, Popal N, Davidson SM, Anderson RH, Scambler PJ (2015). A critical role for the chromatin remodeller CHD7 in anterior mesoderm during cardiovascular development. Dev Biol 405, 82–95.

Rother MB, Pellegrino S, Smith R, Gatti M, Meisenberg C, Wiegant WW, Luijsterburg MS, Imhof R, Downs JA, Vertegaal ACO, *et al*. (2020). CHD7 and 53BP1 regulate distinct pathways for the re-ligation of DNA double-strand breaks. Nat Commun 11, 5775.

Rugh R, Wohlfromm M (1965). Prenatal x-irradiation and postnatal mortality. Radiat Res 26, 493–506.

Schnetz MP, Bartels CF, Shastri K, Balasubramanian D, Zentner GE, Balaji R, Zhang X, Song L, Wang Z, Laframboise T, *et al*. (2009). Genomic distribution of CHD7 on chromatin tracks H3K4 methylation patterns. Genome Res 19, 590–601.

Schnetz MP, Handoko L, Akhtar-Zaidi B, Bartels CF, Pereira CF, Fisher AG, Adams DJ, Flicek P, Crawford GE, Laframboise T, *et al*. (2010). CHD7 targets active gene enhancer elements to modulate ES cell-specific gene expression. PLoS Genet 6, e1001023.

Schulz Y, Wehner P, Opitz L, Salinas-Riester G, Bongers EM, van Ravenswaaij-Arts CM, Wincent J, Schoumans J, Kohlhase J, Borchers A, *et al*. (2014). CHD7, the gene mutated in CHARGE syndrome, regulates genes involved in neural crest cell guidance. Hum Genet 133, 997–1009.

Sperry ED, Hurd EA, Durham MA, Reamer EN, Stein AB, Martin DM (2014). The chromatin remodeling protein CHD7, mutated in CHARGE syndrome, is necessary for proper craniofacial and tracheal development. Dev Dyn 243, 1055–1066.

Torres M, Gómez-Pardo E, Dressler GR, Gruss P (1995). Pax-2 controls multiple steps of urogenital development. Development 121, 4057–4065.

Van Nostrand JL, Brady CA, Jung H, Fuentes DR, Kozak MM, Johnson TM, Lin CY, Lin CJ, Swiderski DL, Vogel H, *et al*. (2014). Inappropriate p53 activation during development induces features of CHARGE syndrome. Nature 514, 228–232.

Vissers LE, van Ravenswaaij CM, Admiraal R, Hurst JA, de Vries BB, Janssen IM, van der Vliet WA, Huys EH, de Jong PJ, Hamel BC, *et al*. (2004). Mutations in a new member of the chromodomain gene family cause CHARGE syndrome. Nat Genet 36, 955–957.

Wang YH, Ho TLF, Hariharan A, Goh HC, Wong YL, Verkaik NS, Lee MY, Tam WL, van Gent DC, Venkitaraman AR, *et al*. (2022). Rapid recruitment of p53 to DNA damage sites directs DNA repair choice and integrity. Proc Natl Acad Sci USA 119, e2113233119.

Ward IM, Minn K, van Deursen J, Chen J (2003). p53 Binding protein 53BP1 is required for DNA damage responses and tumor suppression in mice. Mol Cell Biol 23, 2556–2563.

Whittaker DE, Riegman KL, Kasah S, Mohan C, Yu T, Pijuan-Sala B, Hebaishi H, Caruso A, Marques AC, Michetti C, *et al*. (2017). The chromatin remodeling factor CHD7 controls cerebellar development by regulating reelin expression. J Clin Invest 127, 874–887.

Woodage T, Basrai MA, Baxevanis AD, Hieter P, Collins FS (1997). Characterization of the CHD family of proteins. Proc Natl Acad Sci USA 94, 11472–11477.

Yan S, Thienthanasit R, Chen D, Engelen E, Brühl J, Crossman DK, Kesterson R, Wang Q, Bouazoune K, Jiao K (2020). CHD7 regulates cardiovascular development through ATP-dependent and -independent activities. Proc Natl Acad Sci USA 117, 28847–28858.

Yao H, Hannum DF, Zhai Y, Hill SF, Albanus RD, Lou W, Skidmore JM, Sanchez G, Saiakhova A, Bielas SL, *et al*. (2020). CHD7 promotes neural progenitor differentiation in embryonic stem cells via altered chromatin accessibility and nascent gene expression. Sci Rep 10, 17445.

Zentner GE, Layman WS, Martin DM, Scacheri PC (2010). Molecular and phenotypic aspects of CHD7 mutation in CHARGE syndrome. Am J Med Genet A 152A, 674–686.